Circulating ACE2-expressing Exosomes Block SARS-CoV-2 Infection as an Innate Antiviral Mechanism

Lamiaa El-Shennawy
Northwestern University
Andrew Hoffmann
Northwestern University
Nurmaa Dashzeveg
Northwestern University
Paul Mehl
Northwestern University
Zihao Yu
Northwestern University
Valerie Tokars
Northwestern University
Vlad Nicolaescu
The University of Chicago
Carolina Ostiguin
Northwestern University
Yuzhi Jia
Northwestern University
Lin Li
Northwestern University
Kevin Furlong
The University of Chicago
Chengsheng Mao
Northwestern University
Jan Wysocki
Northwestern University
Daniel Batlle
Northwestern University
Thomas Hope
Northwestern University https://orcid.org/0000-0001-7183-8319
Yang Shen

Texas A&M University
Yuan Luo
Northwestern University
Young Chae
Northwestern University
Hui Zhang
Northwestern University
Suchitra Swaminathan
Northwestern University
Glenn Randall
The University of Chicago
Alexis Demonbreun
Northwestern University
Michael Ison
Northwestern University
Deyu Fang
Northwestern University https://orcid.org/0000-0002-4211-2751
Huiping Liu (**huiping.liu@northwestern.edu**)
Northwestern University https://orcid.org/0000-0003-4822-7995

Letter

Keywords: COVID-19, immunity, angiotensin-converting enzyme 2 (ACE2),ACE2-expressing (ACE2+) exosomes

DOI: https://doi.org/10.21203/rs.3.rs-141729/v1

Abstract

The severe acute respiratory syndrome coronavirus 2 (SARS-CoV-2) causes the coronavirus disease 2019 (COVID-19) with innate and adaptive immune response triggered in such patients by viral antigens. Both convalescent plasma and engineered high affinity human monoclonal antibodies have shown therapeutic potential to treat COVID-19. Whether additional antiviral soluble factors exist in peripheral blood remain understudied. Herein, we detected circulating exosomes that express the SARS-CoV-2 viral entry receptor angiotensin-converting enzyme 2 (ACE2) in plasma of both healthy donors and convalescent COVID-19 patients. We demonstrated that exosomal ACE2 competes with cellular ACE2 for neutralization of SARS-CoV-2 infection. ACE2-expressing ($ACE2^+$) exosomes, but not the ACE2-negative controls, blocked the binding of the viral spike (S) protein RBD to $ACE2^+$ cells in a dose dependent manner, which was 400- to 700-fold more potent than that of vesicle-free recombinant human ACE2 extracellular domain protein (rhACE2). As a consequence, exosomal ACE2 prevented SARS-CoV-2 pseudotype virus tethering and infection of human host cells at a 50–150 fold higher efficacy than rhACE2. A similar antiviral activity of exosomal ACE2 was further demonstrated to block wild-type live SARS-CoV-2 infection. Of note, depletion of $ACE2^+$ exosomes from COVID-19 patient plasma impaired the ability to block SARS-CoV-2 RBD binding to host cells. Furthermore, a dramatic increase in plasma $ACE2^+$ exosome levels were detected in patients with severe COVID-19 pathogenesis. Our data demonstrate that $ACE2^+$ exosomes can serve as a decoy therapeutic and a possible innate antiviral mechanism to block SARS-CoV-2 infection.

Introduction

COVID-19 [1,2] has become a global pandemic resulting in more than 55 million cases and over 1.3 million deaths to date [3]. SARS-CoV-2 shares high structural similarity with SARS-CoV, which caused an outbreak in 2003 [4], and encodes four main proteins- glycoproteins spike (S), envelope (E), membrane (M), and nucleocapsid (N) protein besides several accessory proteins [1,5–7]. Through the external receptor-binding domain (RBD) of the S transmembrane protein, both coronaviruses bind to angiotensin-converting enzyme 2 (ACE2) as a primary receptor for host cell attachment and subsequent entry [1,5–7]. Approaches to block or impede the viral interaction with the entry receptor ACE2 on the host cell, including S-specific neutralization antibodies (Abs) [8–20] and rhACE2 [21–23], inhibit infectivity and prevent COVID-19.

Exosomes are cell-secreted extracellular vesicles (EVs) that participate in a variety of physiological and pathobiological functions [24–28], and present many proteins on the surface reminiscent of their cellular counterpart, such as immune regulators of myeloid and lymphoid cells to affect antiviral immune response [28–30]. Exosomes derived from both plants and human specimen have been used in clinical trials to treat inflammatory diseases and cancers [31–33]. Here, we detected circulating $ACE2^+$ exosomes in plasma from both healthy donors and patients who recovered from COVID-19. Importantly, $ACE2^+$ exosomes inhibit SARS-CoV-2 infection by blocking the viral spike protein binding with its cellular receptor in host cells. Our observations demonstrate that $ACE2^+$ exosomes are a previously unknown

innate antiviral mechanism to prevent SARS-CoV-2 infection, as well as provide a rationale for the use of $ACE2^+$ exosomes to combat COVID-19.

Results

Identification and characterization of $ACE2^+$ exosomes

We previously established an automated and high throughput method, micro flow vesiclometry (MFV), to detect and profile the surface proteins of blood exosomes at single particle resolution [34]. To establish a working protocol for measuring ACE2 expression in exosomes from human plasma, we first determined that ACE2 was detectable in $ACE2^+$ cell-derived exosomes. Two sets of human cell lines HEK-293 (HEK) and HeLa, originally negative for ACE2 ($ACE2^-$ control), were engineered to stably express ACE2 as verified by flow cytometry and immunoblotting (**Fig. 1a & b**). Both $ACE2^+$ cell-and $ACE2^-$ cell-derived exosomes were purified from cell culture supernatants using ultracentrifugation after removal of cell debris and apoptotic bodies (**Extended Fig. S1a**). Exosomes exhibited an average size of approximately 180 nm with equivalent vesicle counts of $6x10^7$ per µg of exosome proteins as measured by nanoparticle tracking analysis (NTA) (**Fig. 1c**). Immunoblotting demonstrated that these exosomes expressed CD63, CD81, and TSG101 but not GRP94 **(Fig. 1b**).

We further developed two cutting-edge platforms: high-resolution cryogenic electron microscopy (cryo-EM) and high-throughput MFV to analyze native exosomes in liquid conditions at single-exosome resolution. Immuno-cryo-EM revealed that both $ACE2^-$ and $ACE2^+$ exosomes have a similar spheric vesicle shape and express CD81 (**Fig. 1d**). More importantly, ACE2 expression was detected in a majority of the imaged vesicles (~ 52% of 178, between 3–40 gold nanoparticles per vesicle) isolated from $ACE2^+$ cells **(Fig. 1d, Extended Fig S1c & d**). MFV also exclusively detected ACE2 in the exosomes derived from both HEK and HeLa cells expressing ACE2, but not from their parental $ACE2^-$ controls, whereas both $ACE2^+$ and $ACE2^-$ cells produced almost equivalent numbers of total EVs ($0.5 \sim 1x10^8$ counts per µg exosome proteins), consistent with the NTA analyses (**Fig. 1c & e, Extended Fig S1e-f**). Within both $ACE2^+$ HEK and HeLa cell-derived exosomes, the $ACE2^+$ exosomes account for up to $1\text{-}5x10^6$ particles per µg of exosome proteins (2–6% of total EVs) (**Fig. 1e, Extended Fig S1f**). Exosomal ACE2 might be under-detected by MFV due to its relatively higher detection threshold than that of cryo-EM images (~ 50% positivity of ACE2) which provide a resolution of single gold nanoparticles stained for ACE2 (**Extended Fig S1d**). The MFV analyses of double stained EVs isolated from HEK-ACE2 and HeLa-ACE2 cells further identified ACE2 largely enriched in $CD81^+$ exosomes (28.6 and 62.5%) or $CD63^+$ exosomes (33.2 and 47.8%) (**Fig. 1f, Extended Fig S1f**).

Taking advantage of the MFV-based direct analysis of circulating exosomes in crude plasma samples, we detected a small subset, ranging from 0.3 to 1.3%, of $ACE2^+$ exosomes in total plasma particles or EVs, which were also enriched in $CD63^+$ exosome subsets from both pre-COVID-19 (NWL-001 and – 004) and COVID-19 (CSB-023 and – 029) patients (**Fig. 1g, Extended Fig S1g).** The ultracentrifugation pellets of

enriched exosomes from plasma specimens had detectable TSG101 and very low ACE2 levels (**Extended Fig. S1h**) further confirming that ACE2$^+$ exosomes exist in plasma from both healthy donors and COVID-19 patients.

ACE2 Exosomes Block SARS-CoV-2 RBD Binding And Viral Infections

To analyze the effects of ACE2$^+$ exosomes on viral infection, we implemented a flow cytometry-based SARS-CoV-2 S protein (RBD)-binding assay (**Extended Fig. S2a**). As expected, ACE2$^+$ HEK cells displayed a specific and high binding (> 90%) with a red fluorophore AF-647-conjugated RBD protein at 16 nM, in contrast to a minimal background level of mock control as well as absent RBD-binding with ACE2$^-$ control cells (**Extended Fig. S2b**). The RBD probe bound to ACE2$^+$ cells in a dose-dependent manner, which was inhibited by pre-incubation with rhACE2 as reported previously [21] (**Fig. 2a & b**). Notably, ACE2$^+$ exosomes inhibited SARS-CoV-2 RBD binding to ACE2$^+$ HEK cells as evidence by the percentage of AF-647$^+$ cells and the mean fluorescence intensity (MFI) which were both dramatically reduced (**Fig. 2a & b**). In contrast, an equal amount of ACE2$^-$ exosomes (20 μg) had negligible effects (**Fig. 2a & b**), indicating that the exosomes inhibit SARS-CoV-2 RBD recognition with their cellular receptors through ACE2. The approximate IC_{50} for soluble rhACE2 to inhibit RBD binding to host cells is 127 nM (~ $7.6x10^{12}$ molecules in 0.1 mL of reaction) (**Fig. 2c**). In order to compare the efficacy between rhACE2 and exosomal ACE2 (exoACE2), we converted the exosome concentrations in exosome particles per measured exosome proteins (~ $1x10^8$/μg) multiplied with estimated number of ACE2 molecules per exosome into molar concentrations of exoACE2. Based on our immune-cryo-EM data, ~ 50% exosomes presenting 3–40 ACE2 molecules (**Extended Fig. S1c-d**), we speculate an average of 20 ACE2 molecules per exosome due to limited exosomal space [35]. Based upon a series of exosome dilution-based RBD neutralization assays, the IC_{50} values of exoACE2 in the exosomes derived from ACE2$^+$ HEK and Hela cells are 0.18 and 0.33 nM, respectively, which contain 1.0-2.0$x10^{10}$ ACE2 molecules in 0.5-1.0$x10^9$ particles (**Fig. 2d-e**). Therefore, exoACE2 possesses 400–700 times better neutralization efficiency than soluble rhACE2 to block SARS-CoV-2 viral RBD binding to human host cells.

Next, we evaluated the neutralization effects of ACE2$^+$ exosomes on the infectivity by SARS-CoV-2 S$^+$ pseudovirus and wild-type virus. When the SIV3-derived SARS-CoV-2 S$^+$ pseudovirus with either a dual Luc2-IRES-Cherry reporter or an eGFP fluorescence protein reporter was utilized, the viral infectivity to ACE2$^+$ host cells was analyzed by flow cytometry of Cherry or eGFP expressing cells as well as luminescence signal of cellular luciferase activity (**Extended Fig. S3a-c**). About 3% of ACE2$^+$ cells were detected with Cherry protein expression when 300 ~ 500 infection-units (IFU) of SARS-CoV-2 S$^+$ pseudoviruses were used, whereas no ACE2$^-$ cells were infected with the same viral dose (**Fig. 3a, Extended Fig. S3d**). ACE2$^+$ exosomes blocked SARS-CoV-2 S$^+$ pseudovirus infection in a dose-dependent manner and achieved more than 90% inhibition at a dose of 20 μg (**Fig. 3b**). A similar result was observed when the SARS-CoV-2 S$^+$ pseudovirus carrying a luciferase reporter was used (**Fig. 3c-e**). The IC_{50} values of exoACE2 in the exosomes derived from ACE2$^+$ HEK and HeLa cells are 12.3 pM and 39.7 pM,

respectively (**Fig. 3c & d**), which are equivalent to 0.4-1.0x10^8 particles (0.37–1.18 μg exosomes) with maximal 0.8-2x10^9 ACE2 molecules in 0.1 mL reactions. In comparison to an IC_{50} of rhACE2 at 1.88 nM (1x10^{11} molecules in 0.1 mL), exosomal ACE2 presents an estimated 50 to 150-fold neutralization efficacy to block SARS-COV-2 infection of human host cells. In contrast, $ACE2^-$ control exosomes only had marginal neutralization effects, which were not dose-dependent (**Fig. 3f & g**). Preincubation of SARS-CoV-2 S^+ pseudovirus with $ACE2^+$ exosomes did not yield infection of ACE2-negative cells (**Extended Fig. S3d**).

Collectively, our results provide a rationale for the use of $ACE2^+$ exosomes as an innovative methodology to prevent SARS-CoV-2 infection. Indeed, upon the wild-type SARS-CoV-2 infection (400 plaque-forming units), HeLa $ACE2^+$ exosomes at the doses of 334 and 668 pM exoACE2 (10 and 20 μg exosomes) protected the vero-6 cells from viral infection-mediated death resulting in an improved host cell viability whereas $ACE2^-$ exosomes failed to protect the cells from viral infection (**Fig. 3h**).

Ace2 Exosomes Associated With Plasma Neutralization Effects

We continued to investigate whether $ACE2^+$ exosome abundancy is associated with viral neutralization effect of human plasma. MFV-based single exosome analysis detected a wide range of $ACE2^+$ exosome abundancy (vesicle counts) in plasma from both pre-COVID-19 (NWL) and convalescent COVID-19 (CSB) patients (**Figs. 1g & 4a)**, implying that the levels of circulating $ACE2^+$ exosomes are variable. As expected, the RBD-IgG levels in COVID-19 patient plasma were significantly associated with their neutralization effects on RBD binding to human cells, but pre-COVID-19 plasma (NWL) had absent or negligible levels of RBD-IgG **(Fig. 4b, Extended Fig. S3e)**.

Together with our discovery that $ACE2^+$ exosome inhibit SARS-CoV-2 infection, we speculated that, in addition to specific neutralization Abs, $ACE2^+$ exosomes might function as an innate anti-SARS-COV-2 mechanism. To investigate this idea, we first enriched plasma exosomes by ultracentrifugation (**Fig. 4c & d**). Importantly, $ACE2^+$ exosomes pelleted from the plasma of both healthy donors and COVID-19 patients partially inhibited RBD-binding to ACE2-expressing HEK cells (**Fig. 4e**). To validate whether the $ACE2^+$ exosomes in the plasma pellet were responsible for inhibition of RBD binding, we used RBD-conjugated magnetic beads to deplete the majority of $ACE2^+$ exosomes in the samples (**Fig. 4c & d**). Depletion of $ACE2^+$ exosomes significantly impaired the ability of plasma samples to inhibt RBD-binding to $ACE2^+$ HEK cells (**Fig. 4e**), indicating that the $ACE2^+$ exosomes in the plasma from both healthy donors and COVID-19 patients were responsible for anti-SARS-CoV-2 activity.

We also noticed that the pellets from one COVID-19 plasma (CSB-012) had residual but detectable levels of RBD-specific IgG, which were also depleted by RBD-beads (**Fig. 4c & f**). This implies that IgG may contribute to the neutralization capacity of the plasma pellets from COVID-19 patients, but not the healthy donors, to suppress SARS-CoV-2 infectivity. Based on the altered $ACE2^+$ exosome levels (vesicle counts measured by MFV) in all four samples and the RBD-IgG alteration in CSB-012 and CSB-024, we adapted a mathematical model to estimate the individual and relative contributions of $ACE2^+$ exosomes and RBD-

IgG in convalescent plasma to block SARS-CoV-2 binding (**Extended Fig. S3e-f**). Adjusted R^2, a commonly used measure for model's goodness-of-fit, indicates how much of the outcome is being explained by regression factors while also adjust the number of explanatory factors in a model by certain penalty. The multivariable linear regression[36,37] of RBD neutralization activity of COVID-19 patient plasma on RBD-IgG level only results in an adjusted R^2 of 0.623 (**Extended Fig. S3e**), while similar regression on both $ACE2^+$ exosomes and RBD-IgG levels presents an adjusted R^2 of 0.679 (**Fig. 4g**). Analysis of variance suggested the latter one, i.e. adding $ACE2^+$ exosomes to the model to explain RBD neutralization activity of COVID-19 patient plasma, significantly improved the model fitting ($p = 0.027$). In addition, the Lindeman-Merenda-Gold analysis[36] suggested that, among the total model fitting contribution, ACE2 counts 6.7% of it, while anti-RBD IgG contributed 93.3%. However, the 6.7% by ACE2 is not ignorable ($p = 0.027$). These results imply a potential antiviral contribution of circulating $ACE2^+$ exosomes.

Importantly, a significant higher level of circulating $ACE2^+$ exosomes were detected in the plasma of hospitalized patients or those in intensive care units (ICU) *versus* that of the outpatients (**Fig. 4h-i, Extended Fig. S4**), suggesting that the $ACE2^+$ exosomes levels can be potentially regulated by either the SARS-CoV2 virial load or the associated pathogenesis, or both. Taken together, our data reveal a previously unknown antiviral mechanism of circulating $ACE2^+$ exosomes that may suppress infection by SARS-CoV-2 and other viruses utilizing ACE2 as an entry receptor.

Discussion

Our studies demonstrate that $ACE2^+$ exosomes can compete with host cell surface ACE2 to inhibit SARS-CoV-2 infection, and possibly by other coronaviruses that utilize ACE2 as their initial tethering receptor. Similarly, a recent study has shown that rhACE2 inhibits SARS-CoV-2 infection [21]. Based on an assumption that one exosome is capable of containing a limited number of total protein molecules [35] and our cryo-EM data showing possibly up to 20 ACE2 molecules per exosome, exosomal ACE2 might possess at least a 100-fold better efficiency to block SARS-CoV-2 infection than soluble rhACE2.

Beyond a significant amplification of exosomal ACE2 in the anti-SARS-CoV-2 efficacy in comparison to the purified rhACE2 proteins or its Fc-fusions [38], we anticipate that the therapeutic efficacy of $ACE2^+$ exosomes can be further potentiated through co-delivering additional anti-SARS-CoV-2 medicines, such as remdesivir [39,40]. Exosomes have been utilized as drug delivery systems with therapeutic potential against various disorders including infectious diseases and cancers [41,42]. Of note, exosomes derived from both plants and human specimen, such as dendritic cells and tumor cells, have been evaluated in multiple clinical trials and proven safe in human [31–33]. For example, cancer cell-derived exosomes containing chemo drugs, in addition to neo-antigens have been used to treat patients diagnosed with malignant pleural effusion (NCT01854866 and NCT02657460). The exosomes derived from plans, including grape (NCT01668849) and ginger or aloe (NCT03493984), have been registered in clinical trial in treating diseases due to radiation- and chemotherapy-induced oral mucositis.

In addition, circulating exosomes in plasma represent an important component of blood in terms of its defensive, homeostatic and signal transduction properties [28–30, 34]. Importantly, here we detected a substantial amount of $ACE2^+$ exosomes in human plasma, and $ACE2^+$ exosomes function as a potent decoy to protect host cells from SARS-CoV-2 infection. Our discovery reveals that circulating $ACE2^+$ exosomes may serve as a previously unknown innate antiviral mechanism to protect the host from coronavirus infection. More interestingly, the levels of this innate antiviral ACE2 exosomes appear to be regulated because we detected an 2–3 folds increase in the average levels of the circulating $ACE2^+$ exosomes in COVID-19 patients with severe disease. It has been well established that the clinical disease severity may be positively associated with higher SARS-CoV-2 virial load[43], implying a possibility that either the virial pathogens, or their associated pathogenesis, induce $ACE2^+$ exosome generation. Future studies are needed to investigate whether circulating ACE2 exosomes account for reduced SARS-CoV-2 viral load and COVID-19 pathogenesis, as well as how SARS-CoV2 infection regulates the levels of $ACE2^+$ exosomes.

Methods

Human subject study and biosafety approvals.

All research activities with human blood specimens of pre-COVID-19 and COVID-19 convalescent patients were implemented under NIH guidelines for human subject studies and the protocols approved by the Northwestern University Institutional Review Board (STU00205299 and #STU00212371) as well as the Institutional Biosafety Committee.

Cell culture

The parent $ACE2^-$ human embryonic kidney HEK-293 cells (HEK) or human cervical cancer HeLa cells (HeLa) are transduced with lentiviral pDual-ACE2 expression vector for stable ACE2 expression and production of $ACE2^+$ exosomes. Dr. Thomas Gallagher of Stritch Medical School, Loyola University kindly provided HeLa and HeLa-ACE2 cells via the Hope group. ACE2- parent cell serve as negative controls in production of ACE2- exosomes in the culture. Cells were tested for mycoplasma contamination before culturing. Cells were grown in Dulbecco's Modified Eagle's Medium (DMEM) supplemented with 10% (v/v) fetal bovine serum (FBS), 100 U/mL penicillin and 100 mg/mL streptomycin. FBS used to prepare complete media was exosome-depleted by ultracentrifugation at 100,000 × *g* for 16 h at 4 °C.

Flow cytometry

Cells were blocked with mouse serum IgG (Sigma, 15381) for 10 min at room temperature and then incubated with specific antibodies; AF-647 mouse anti-human ACE2 (R&D systems, FAB9332R), AF-488 mouse anti-human ACE2 (R&D systems, FAB9333G), AF-647 isotype control mouse IgG2b (R&D systems, IC003R) or AF-488 isotype control mouse IgG2bAF488 (R&D systems, IC003G) for 45 min on ice, followed

by washing twice with 2% exosome-free FBS/PBS. Finally, the cells were diluted in 2% exo-free FBS/PBS and analyzed on a BD-LSR II flow cytometer (BD Biosciences).

Isolation and Purification of cell line-derived exosomes

Exosomes were isolated from the cell culture supernatant of each of the four cell lines as described previously[44]. Cells were cultured as monolayers for 48-72 h under an atmosphere of 5% CO_2 at 37 °C. When cells reached confluency of approximately 80-90%, culture supernatant was collected, and exosomes were isolated using differential centrifugation. First, the supernatant was centrifuged at 2,000 × g for 10 min then at 10,000 × g for 30 min to remove dead cells and cell debris. Second, the supernatant was ultracentrifuged for 70 min at 100,000 × g to pellet the exosomes. Exosomes were then washed by resuspension in 30 mL of sterile PBS (Hyclone, Utah, USA), and pelleted by ultracentrifugation for 70 h at 100,000 × g. The exosome pellet was resuspended in 100 µl PBS and stored at −80 °C.

Western blotting

Cells and exosomes were lysed by RIPA buffer with protease inhibitor cocktail (1:100 dilution) for 30 min on ice, then centrifuged for 15 min at 4 °C and 14,000 rpm. 10-20 µg of cell-derived proteins and 2-8 µg of exosome-derived proteins were denatured at 100 °C for 5 min and loaded to SDS-PAGE, then transferred to PVDF membranes. The antibodies, ACE2 (R&D systems, AF933), CD81 (GeneTex, CTX101766), CD63 (Proteintech, 25682-1-AP), GRP94 (Proteintech, 1H10B7), TSG101 (Proteintech, 14497-1-AP) and β-actin (Sigma, A5441) were used as primary antibodies and horseradish peroxidase (HRP)-conjugated secondary antibodies were from Promega (Rabbit W401B and Mouse W402B), and the substrate ECL was detected by Pierce ECL2 solution (Thermo Fisher Scientific, 1896433A).

Nanoparticle tracking analysis

Analysis was performed at the Analytical bioNanoTechnology Core Facility of the Simpson Querrey Institute at Northwestern University. All samples were diluted in PBS to a final volume of 1 ml and ideal measurement concentrations were found by pre-testing the ideal particle per frame value. Settings were according to the manufacturer's software manual (NanoSight NS3000).

Micro Flow Vesiclometry (MFV) Analysis of Exosomes

Antibody solutions were centrifuged at 14000 × g for 1 h at 4 °C to remove aggregates before use. Exosomes (1-2 µg protein equivalent amount of exosomes in 20 µL of PBS) were blocked using 1µg of mouse serum IgG for 10 min at RT then incubated with: AF-488 mouse anti-human ACE2 (R&D systems, FAB9333G), APC mouse antihuman CD81 (BD Biosciences, 561958), AF-647 mouse antihuman CD63 (BD, Biosciences, 561983), AF-488 isotype control mouse IgG2b (R&D systems, IC003G), APC isotype control mouse $IgG_1κ$ (BD Biosciences, 555751) or AF-647 isotype control mouse $IgG_1κ$ (BD, Biosciences, 557714) for 45 min at 4°C. The solution was then diluted to 200µL with PBS and the samples were run on Apogee A50 Micro Flow Cytometer (MFC) (Apogee Flow Systems, Hertfordshire, UK)

(http://www.apogeeflow.com/products.php). The reference ApogeeMix beads (Apogee Flow Systems, 1493), were used to assess the performance of Apogee MFC, and to compare the size distribution of the exosomes. PBS was run as a background control.

Immuno-cryo-EM imaging

Antibody solutions and other staining buffers were centrifuged to remove non-specific particles or aggregates in the buffer of intereat, at 14000 × g for 1 h at 4 °C before use. Exosomes (10µg in 100uL) were blocked using 5µg of mouse serum IgG for 10 min at RT then incubated with mouse anti-human ACE2 (R&D systems, FAB9333G), mouse antihuman CD81 (BD Biosciences, 551108), isotype control mouse IgG2b (R&D systems, IC003G) or isotype control mouse $IgG_1κ$ (BD Biosciences, 551954) for 45 min at 4 °C.. To rinse samples, 1mL PBS was added to the tubes, and exosomes were centrifuged 100,000 × g for 30 min at 4°C. PBS was aspirated, samples were reconstituted in 100 uL PBS, and incubated with EM goat anti-mouse IgG (H&L) 10 nm gold conjugated (BBI solutions, EM.GMHL10) (7:100) for 30 min at RT. Exosomes were then rinsed by adding 1300 uL PBS then centrifugation 100,000 × g for 15 min at 4°C. Finally, PBS was aspirated, and exosomes were reconstituted in 50 uL PBS.

For cryoEM visualization, samples were prepared from freshly stained exosomes at the concentration provided. For cryo-freezing, 3.5µl of exosome solutions were applied to fresh glow-discharged (10 s, 15 mA; Pelco EasiGlow) lacey carbon TEM grids (Electron Microscopy Services) and vitrified using a FEI Vitrobot Mark IV (FEI, Hillsboro, OR). The sample was applied to the grid and kept at 85% humidity and 10 oC. After a 10 s incubation period the grid was blotted with Whatman 595 filter paper for 4 seconds using a blot force of 5 and plunge frozen into liquid ethane. Samples were imaged using a JEOL 3200FS electron microscope equipped with an omega energy filter operated at 200 kV with a K3 direct electron detector (Ametek) using the minimal dose system. The total dose for each movie was ~20 e-/A2 and was fractionated into 14 frames at a nominal magnification between 8,000 to 15,000 (pixel size on the detector between 4.1 Å to 2.2 Å, respectively). After motion correction of the movies [45], exosomes were identified manually using ImageJ [46]. Two grids were prepared and imaged with 10-20 fields for each condition.

Development of the SARS-Cov-2 RBD “bait”:

RBD of 223 amino acid (Arg319-Phe541) fragment of the SARS-CoV-2 Spike protein that binds to the ACE2 receptor (Raybiotech, 230-30162-100) was biotinylated using NHS-PEG4-Biotin (Thermo Fisher, 21330). The protein was de-salted using Zeba Quick Spin columns (Thermo Fisher, 89849) and incubated with Streptavidin-AlexaFluor-647 (SA-AF-647) (Thermo Fisher, S21374) to make the RBD-biotin-AF647 bait.

Cell-based RBD binding neutralization by $ACE2^+$ exosomes and human plasma

The RBD-biotin-AF647 bait (3.3 and 16 nM) was incubated with exosomes ($ACE2^+$ and $ACE2^-$), recombinant human ACE2 extracellular region (rhACE2, RayBiotech, 230-30165), or human plasma (10 µl

or 80 µl) for 45 minutes on ice (creating “neutralized RBD”), then incubated with $ACE2^+$ HEK-293 cells (200,000 cells in 100 µL) for 45 minutes on ice. Human recombinant ACE2 protein was used as a positive control (70-140 ng). RBD bait that was incubated with PBS, or with $ACE2^-$ exosomes, non-fluorescent RBD bait (mock control) and $ACE2^-$ cells were used as controls. Cells were then spun and washed twice with PBS. DAPI was added as to exclude dead cells analyzed on flow cytometer and viable singlets were gated for percentage and mean fluorescence intensity (MFI) measurements of the RBD-$AF647^+$ population.

Neutralization effects of $ACE2^+$ exosomes on SARS-CoV-2 $spike^+$ pseudovirus infection to human host cells.

The SARS-CoV-2 spike (S^+) pseudovirus carrying the Luc2-Cherry reporters were made for live virus neutralization assay after the pcDNA3-spike expression vector was transfected along with pCMV-Luc2-IRES-Cherry and pSIV3+ lentiviral vectors into a lentivirus producing cell HEK-293. The S^+ pseudovirus was then incubated with $ACE2^+$ exosomes, or $ACE2^-$ exosomes, or a positive control rhACE2, or negative control (PBS), for 1 hr at 37^{o}C prior to the infection with $ACE2^+$ human host cells HeLa in 96-well plates (5,000 cells/well). A bald virus without spike expression and ACE^- cells served as negative controls. Flow cytometry of Cherry or eGFP and luciferase activity analysis (Promega, E1500) were used to assess viral infectivity.

Wild-type SARS-CoV-2 live virus infection to vero-6 cells at the BSL3 facility

The wild-type SARS-CoV-2 live virus study was conducted at the BSL-3 facility at the NIAID-supported University of Chicago Howard T. Ricketts Regional Biochontainment Laboratory. One day prior to viral infections, 10,000 vero-6 cells were seeded per well in triplicates onto 96-well plates. 16 hours after seeding, the attached cells were infected with mock controls (no virus) and wild-type SARS-CoV-2 (500 pfu) viruses which were pre-mixed with a serial of doses of exosomes (starting from 20 µg with 6 times of 1:2 dilutions) or an untreated control. 96 hours later, the host cell viability (opposite to viral infectivity-caused cell death) was measured by crystal violet staining which stained attached viable cells on the plate following fixation. Cells killed off by the virus were floating and excluded. For the untreated control, the cells were infected but left without any treatment with a value of maximal cell death caused by the virus. The second control was the mock infected control where cells grew in the absences of virus or experimental sample representing the maximum normal cell growth over the time period. The absorbance value of the untreated control was subtracted from all other absorbance values thereby making untreated 0 then all absorbance values were divided by the mock infected value thereby making that value 100.

RBD-IgG quantitative ELISA assay

The ELISA protocol was validated as previously described [47,48] and used herein with the modification of using plasma instead of serum. Plasma samples were diluted by half with PBS during RosetteSep human B cell processing (StemCell Technologies #15064), aliquoted, and stored at -80C until analysis. Plasma was run in quadruplicate and reported as the average. Results were normalized to the CR3022

antibody with known affinity to RBD of SARS-CoV-2 [49]. Sample anti-RBD IgG concentration reported as μg/ml was calculated from the 4PL regression of the CR3022 calibration curve. A sample value >0.39 μg/ml CR3022 was considered seropositive.

Exosome enrichment by ultracentrifuge

Covid-19 (CSB) and pre-COVID-19 (NWL) patient derived plasma samples were obtained from Northwestern Memorial Hospital and stored at -80 °C. CSB and NWL plasmas were ultra-centrifuged (Beckman Coulter) at 100000 x g for 2, 4, 8 and 18 h at 4 °C to isolate and enrich exosomes in the pellets. After centrifuge, supernatants and plasma pellets were collected separately. Plasma pellets were resuspended in appropriate volumes of PBS. The levels of $ACE2^+$ exosomes in plasma samples were evaluated by MFV on Apogee and western blotting using exosome marker TSG101 and ACE2. $ACE2^+$ cell line derived exosomes were used as a positive control.

Depletion of $ACE2^+$ exosomes by RBD-beads

CSB and NWL patient plasma samples (1.0-2.0 ml) were ultra-centrifuged for 8 h at 100000 x g at 4 °C, and the pellets were resuspended in 250-500 μL PBS as exosome-enriched samples for subsequent bead-mediated depletion. RBD-coupled magnetic beads or anti ACE2-coupled dynabeads beads were prepared according to manufacturer's protocols. Biotin conjugated RBD protein (ACROBiosystems, SPD-C82E9) were coupled with magnetic beads (CELLection Biotin Binder Kit, Thermo Fisher Sceintific, 11533D), and 5 μg of anti-ACE2 antibody (R&D systems, AF933) or isotope control IgG (R&D systems) were conjugated to dynabeads (Dynabeads Co-Immunoprecipitation Kit, Thermo Fisher Scientific, 14321D). Exosome pellet samples were incubated with the beads for overnight at 4°C and then the beads were removed by spinning or magnetic forces. The $ACE2^+$ exosome depletion efficiency was confirmed by MFV on Apogee and/or western blotting methods.

The altered neutralization effects of NWL and CSB plasma-enriched exosomes (resuspended pellets) prior to and after bead depletion were measured via flow cytometry as modified RBD binding to human host cells as described above. And rhACE2 protein (RayBiotech, 230-30165) was used as a positive control (70-140 ng).

Patient association analyses

Circulating exosomal $ACE2^+$ counts, RBD-IgG levels, plasma neutralization on RBD binding, and clinical data were collected from the laboratory and Northwestern EDW database, electronically recorded, and verified by laboratory staff. There were in total n=30 measurable data points for final statistical analyses. To reduce bias resulting from batch effects, four independent replications on RBD-IgG test were performed in the laboratory. Therefore, one-way ANOVA was performed to compare group means and it suggests that the replications did not show statistically significant batch or measure errors ($F=0.01$, p-value>0.9), thus, mean values of the replications were taken for analysis. In addition, log-linear model (Poisson regression) was fitted to estimate the associations between normalized percentage (%) of RBD

binding to cells and independent predictors of interest. It suggested negative associations (see Fig. 4g and extended Fig. 4e) and the adjusted R^2 suggests that the combined circulating $ACE2^+$ exosome counts + RBD-IgG level explains the relation better than RBD-IgG alone (Adj. R^2 =0.623 p<0.0001). Following linear modeling to determine that combined $ACE2^+$ exosomes + RBD-IgG explains the relation better than RBD alone, relative importance of $ACE2^+$ exosomes as compared to anti-RBD IgG was calculated using the Lindeman, Merenda and Gold (1980)[36] formula using the 'relaimpo' package in R (Grömping, 2006)[37]. Metrics were normalized to sum to 100%. Coeffecient from this analysis was used to create graphs in Fig 4g. All statistical analyses were performed by R 4.0.2.

Other Statistical Analysis

GraphPad Prism 6.0 Software was used to perform statistical analyses and calculate the $IC_{50.}$ One way or two ways ANOVA (followed by Tukey or Sidak's posttest) were used where appropriate. Data are presented as mean ± standard deviation (SD).

Declarations

Acknowledgments

We are thankful to the team of Northwestern COVID-19 Antibody and Cancer Collaborative Group (U54 and U18 Prep Team) and advisory members with their scientific input and resourceful support for the project, especially Drs. Alfred L. George Jr. who also edited our manuscript, James Crowe, Judith Varner, Richard D'Aquila, Leonidas C. Platanias, Rex L. Chishom, Alan R. Hauser, Elizabeth M. McNally, and William A. Muller. The work was partially funded by Northwestern University Feinberg School of Medicine Emerging and Re-emerging Pathogens Program (EREPP) (H.L.), Department of Pharmacology Start-up fund (H.L.), and the R.H. Lurie Comprehensive Cancer Center Blood Biobank fund (M.I.). We gratefully acknowledge the support from the R.H. Lurie Comprehensive Cancer Center Structural Biology Facility and Flow Core. The Ametek K3 DDE at Northwestern University for cryo-EM was generously provided by Professor Robert A. Lamb, Ph.D., Sc.D., HHMI investigator. The ACE2-expressing HeLa cells were provided by Dr. Thomas Gallagher of Stritch Medical School, Loyola University. We appreciate the effort of BSL-3 facility at the NIAID-supported University of Chicago Howard T. Ricketts Regional Biochontainment Laboratory for performing the wild-type SARS-CoV-2 live virus study.

References

1 Zhou, P. *et al.* A pneumonia outbreak associated with a new coronavirus of probable bat origin. *Nature* **579**, 270-273, doi:10.1038/s41586-020-2012-7 (2020).

2 Zhu, N. *et al.* A Novel Coronavirus from Patients with Pneumonia in China, 2019. *The New England journal of medicine* **382**, 727-733, doi:10.1056/NEJMoa2001017 (2020).

3 Rothan, H. A. & Byrareddy, S. N. The epidemiology and pathogenesis of coronavirus disease (COVID-19) outbreak. *J Autoimmun* **109**, 102433, doi:10.1016/j.jaut.2020.102433 (2020).

4 Li, W. *et al.* Bats are natural reservoirs of SARS-like coronaviruses. *Science* **310**, 676-679, doi:10.1126/science.1118391 (2005).

5 Hoffmann, M. *et al.* SARS-CoV-2 Cell Entry Depends on ACE2 and TMPRSS2 and Is Blocked by a Clinically Proven Protease Inhibitor. *Cell*, doi:10.1016/j.cell.2020.02.052 (2020).

6 Wrapp, D. *et al.* Cryo-EM structure of the 2019-nCoV spike in the prefusion conformation. *Science (New York, N.Y* **367**, 1260-1263, doi:10.1126/science.abb2507 (2020).

7 Yan, R. *et al.* Structural basis for the recognition of the SARS-CoV-2 by full-length human ACE2. *Science (New York, N.Y*, doi:10.1126/science.abb2762 (2020).

8 Mullard, A. First antibody against COVID-19 spike protein enters phase I. *Nat Rev Drug Discov* **19**, 435, doi:10.1038/d41573-020-00108-x (2020).

9 Bost, P. *et al.* Host-Viral Infection Maps Reveal Signatures of Severe COVID-19 Patients. *Cell* **181**, 1475-1488 e1412, doi:10.1016/j.cell.2020.05.006 (2020).

10 Chi, X. *et al.* A neutralizing human antibody binds to the N-terminal domain of the Spike protein of SARS-CoV-2. *Science (New York, N.Y*, doi:10.1126/science.abc6952 (2020).

11 Baum, A. *et al.* Antibody cocktail to SARS-CoV-2 spike protein prevents rapid mutational escape seen with individual antibodies. *Science (New York, N.Y*, doi:10.1126/science.abd0831 (2020).

12 Liu, A., Li, Y., Peng, J., Huang, Y. & Xu, D. Antibody responses against SARS-CoV-2 in COVID-19 patients. *Journal of medical virology*, doi:10.1002/jmv.26241 (2020).

13 Long, Q. X. *et al.* Antibody responses to SARS-CoV-2 in patients with COVID-19. *Nat Med* **26**, 845-848, doi:10.1038/s41591-020-0897-1 (2020).

14 Wu, Y. *et al.* A noncompeting pair of human neutralizing antibodies block COVID-19 virus binding to its receptor ACE2. *Science (New York, N.Y* **368**, 1274-1278, doi:10.1126/science.abc2241 (2020).

15 Brouwer, P. J. M. *et al.* Potent neutralizing antibodies from COVID-19 patients define multiple targets of vulnerability. *Science (New York, N.Y*, doi:10.1126/science.abc5902 (2020).

16 Rogers, T. F. *et al.* Isolation of potent SARS-CoV-2 neutralizing antibodies and protection from disease in a small animal model. *Science (New York, N.Y*, doi:10.1126/science.abc7520 (2020).

17 Hansen, J. *et al.* Studies in humanized mice and convalescent humans yield a SARS-CoV-2 antibody cocktail. *Science (New York, N.Y*, doi:10.1126/science.abd0827 (2020).

18 Shi, R. *et al.* A human neutralizing antibody targets the receptor-binding site of SARS-CoV-2. *Nature*, doi:10.1038/s41586-020-2381-y (2020).

19 Ju, B. *et al.* Human neutralizing antibodies elicited by SARS-CoV-2 infection. *Nature*, doi:10.1038/s41586-020-2380-z (2020).

20 Chen, X. *et al.* Human monoclonal antibodies block the binding of SARS-CoV-2 spike protein to angiotensin converting enzyme 2 receptor. *Cell Mol Immunol* **17**, 647-649, doi:10.1038/s41423-020-0426-7 (2020).

21 Monteil, V. *et al.* Inhibition of SARS-CoV-2 Infections in Engineered Human Tissues Using Clinical-Grade Soluble Human ACE2. *Cell*, doi:10.1016/j.cell.2020.04.004 (2020).

22 Batlle, D., Wysocki, J. & Satchell, K. Soluble angiotensin-converting enzyme 2: a potential approach for coronavirus infection therapy? *Clin Sci (Lond)* **134**, 543-545, doi:10.1042/CS20200163 (2020).

23 Davidson, A. M., Wysocki, J. & Batlle, D. Interaction of SARS-CoV-2 and Other Coronavirus With ACE (Angiotensin-Converting Enzyme)-2 as Their Main Receptor: Therapeutic Implications. *Hypertension* **76**, 1339-1349, doi:10.1161/HYPERTENSIONAHA.120.15256 (2020).

24 Thery, C., Zitvogel, L. & Amigorena, S. Exosomes: composition, biogenesis and function. *Nat Rev Immunol* **2**, 569-579, doi:10.1038/nri855 (2002).

25 Stoorvogel, W., Kleijmeer, M. J., Geuze, H. J. & Raposo, G. The biogenesis and functions of exosomes. *Traffic* **3**, 321-330, doi:10.1034/j.1600-0854.2002.30502.x (2002).

26 Costa-Silva, B. *et al.* Pancreatic cancer exosomes initiate pre-metastatic niche formation in the liver. *Nat Cell Biol* **17**, 816-826, doi:10.1038/ncb3169 (2015).

27 Peinado, H. *et al.* Melanoma exosomes educate bone marrow progenitor cells toward a pro-metastatic phenotype through MET. *Nat Med* **18**, 883-891, doi:10.1038/nm.2753 (2012).

28 Kamerkar, S. *et al.* Exosomes facilitate therapeutic targeting of oncogenic KRAS in pancreatic cancer. *Nature* **546**, 498-503, doi:10.1038/nature22341 (2017).

29 Chen, G. *et al.* Exosomal PD-L1 contributes to immunosuppression and is associated with anti-PD-1 response. *Nature* **560**, 382-386, doi:10.1038/s41586-018-0392-8 (2018).

30 Poggio, M. *et al.* Suppression of Exosomal PD-L1 Induces Systemic Anti-tumor Immunity and Memory. *Cell* **177**, 414-427 e413, doi:10.1016/j.cell.2019.02.016 (2019).

31 Murphy, D. E. *et al.* Extracellular vesicle-based therapeutics: natural versus engineered targeting and trafficking. *Exp Mol Med* **51**, 1-12, doi:10.1038/s12276-019-0223-5 (2019).

32 Mendt, M. *et al.* Generation and testing of clinical-grade exosomes for pancreatic cancer. *JCI Insight* **3**, doi:10.1172/jci.insight.99263 (2018).

33 Chen, L., Xiang, B., Wang, X. & Xiang, C. Exosomes derived from human menstrual blood-derived stem cells alleviate fulminant hepatic failure. *Stem Cell Res Ther* **8**, 9, doi:10.1186/s13287-016-0453-6 (2017).

34 Kibria, G. *et al.* A rapid, automated surface protein profiling of single circulating exosomes in human blood. *Sci Rep* **6**, 36502, doi:10.1038/srep36502 (2016).

35 Vlassov, A. V., Magdaleno, S., Setterquist, R. & Conrad, R. Exosomes: current knowledge of their composition, biological functions, and diagnostic and therapeutic potentials. *Biochimica et biophysica acta* **1820**, 940-948, doi:10.1016/j.bbagen.2012.03.017 (2012).

36 Lindeman, R. M., PF; Gold, RZ. Introduction to bivariate and multivariate analysis. *Vereniging voor Statistiek Bulletin* **14**, 11–14 (1980).

37 Groemping, U. Relative Importance for Linear Regression in R: The Package relaimpo. *2006* **17**, 27, doi:10.18637/jss.v017.i01 (2006).

38 Linsky, T. W. *et al.* De novo design of potent and resilient hACE2 decoys to neutralize SARS-CoV-2. *Science* **370**, 1208-1214, doi:10.1126/science.abe0075 (2020).

39 Tu, Y. F. *et al.* A Review of SARS-CoV-2 and the Ongoing Clinical Trials. *Int J Mol Sci* **21**, doi:10.3390/ijms21072657 (2020).

40 Ison, M. G., Wolfe, C. & Boucher, H. W. Emergency Use Authorization of Remdesivir: The Need for a Transparent Distribution Process. *JAMA* **323**, 2365-2366, doi:10.1001/jama.2020.8863 (2020).

41 Kibria, G., Ramos, E. K., Wan, Y., Gius, D. R. & Liu, H. Exosomes as a Drug Delivery System in Cancer Therapy: Potential and Challenges. *Mol Pharm* **15**, 3625-3633, doi:10.1021/acs.molpharmaceut.8b00277 (2018).

42 Roefs, M. T., Sluijter, J. P. G. & Vader, P. Extracellular Vesicle-Associated Proteins in Tissue Repair. *Trends Cell Biol*, doi:10.1016/j.tcb.2020.09.009 (2020).

43 Walsh, K. A. *et al.* SARS-CoV-2 detection, viral load and infectivity over the course of an infection. *J Infect* **81**, 357-371, doi:10.1016/j.jinf.2020.06.067 (2020).

44 Harding, C. V., Heuser, J. E. & Stahl, P. D. Exosomes: looking back three decades and into the future. *J Cell Biol* **200**, 367-371, doi:10.1083/jcb.201212113 (2013).

45 Zivanov, J. *et al.* New tools for automated high-resolution cryo-EM structure determination in RELION-3. *Elife* **7**, doi:10.7554/eLife.42166 (2018).

46 Schneider, C. A., Rasband, W. S. & Eliceiri, K. W. NIH Image to ImageJ: 25 years of image analysis. *Nat Methods* **9**, 671-675, doi:10.1038/nmeth.2089 (2012).

47 Amanat, F. *et al.* A serological assay to detect SARS-CoV-2 seroconversion in humans. *medRxiv : the preprint server for health sciences*, doi:10.1101/2020.03.17.20037713 (2020).

48 McDade, T. W. *et al.* High seroprevalence for SARS-CoV-2 among household members of essential workers detected using a dried blood spot assay. *PloS one* **15**, e0237833, doi:10.1371/journal.pone.0237833 (2020).

49 Yuan, M. *et al.* A highly conserved cryptic epitope in the receptor binding domains of SARS-CoV-2 and SARS-CoV. *Science (New York, N.Y.)* **368**, 630-633, doi:10.1126/science.abb7269 (2020).

Figures

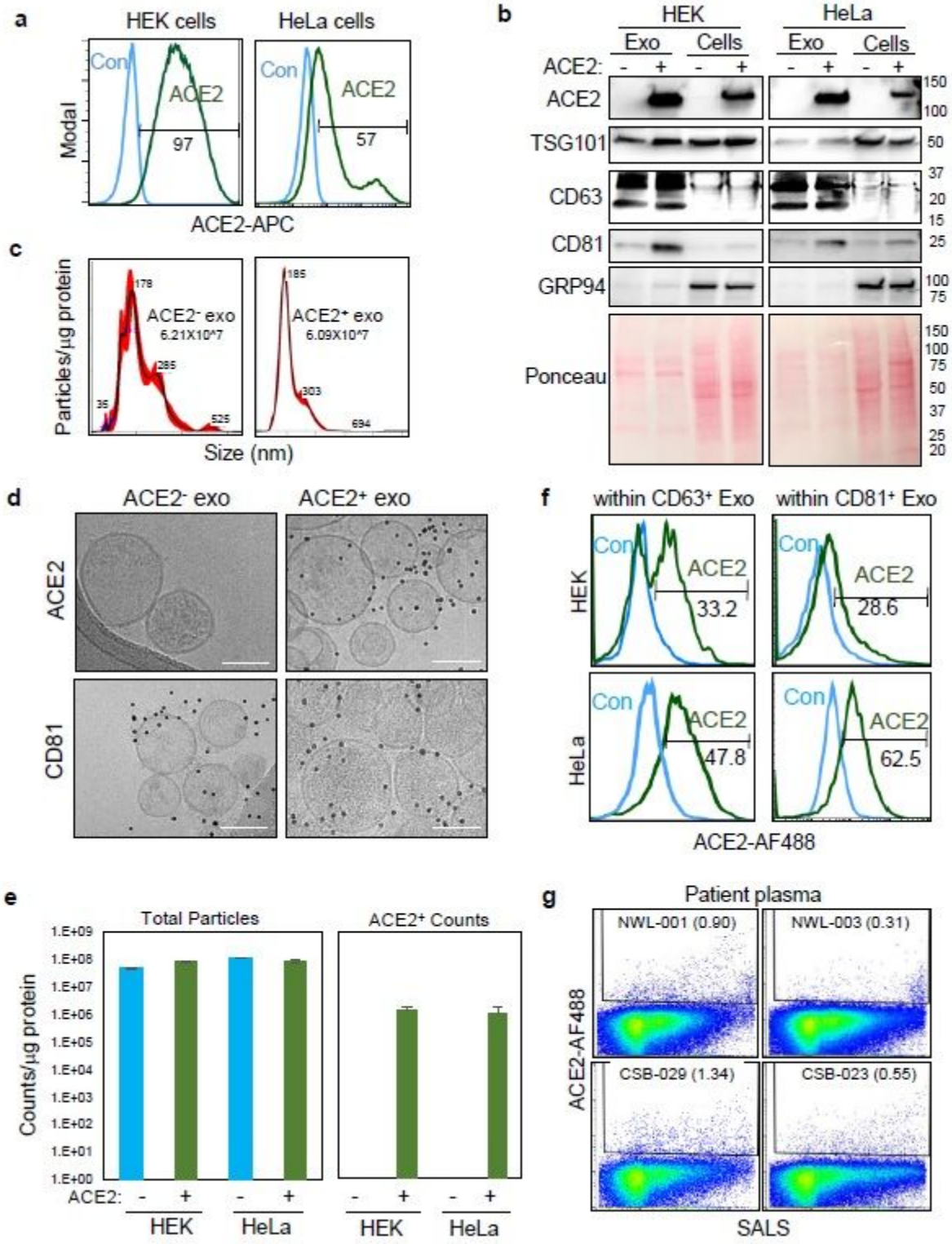

Figure 1

a Flow profiles of ACE 2 expression in HEK and HeLa parental control cells (light blue line, ACE 2 and with ACE 2 overexpression (ACE 2 green line) b Immunoblots of HEK and HeLa (ACE 2 and ACE 2 exosomes and cell lysates for ACE 2 TSG 101 CD 63 CD 81 GRP 94 and loading control of the membrane proteins upon Ponceau staining c Nanosight based NTA analysis of the sizes of HEK derived ACE 2 and ACE 2 exosomes e Cryo EM images of HEK derived ACE 2 –(and ACE 2 ++(exosomes stained with ACE 2

(and CD 81 (bottom panels Scale bars= 100 nm eQuantified counts of Apogee MFV based total extracellular vesicles (and ACE 2 exosomes f Overlay flow profiles of ACE 2 positivity within CD 81 ++(left panels) and CD 63 ++(right panels) exosomes isolated from HEK ACE 2 (top panels) and HeLa ACE 2 (bottom panels) cells, respectively g MFV detection of circulating ACE 2 exosomes in human plasma of pre COVID 19 (NWL 001 and 003 and COVID 19 (CSB 029 and 023

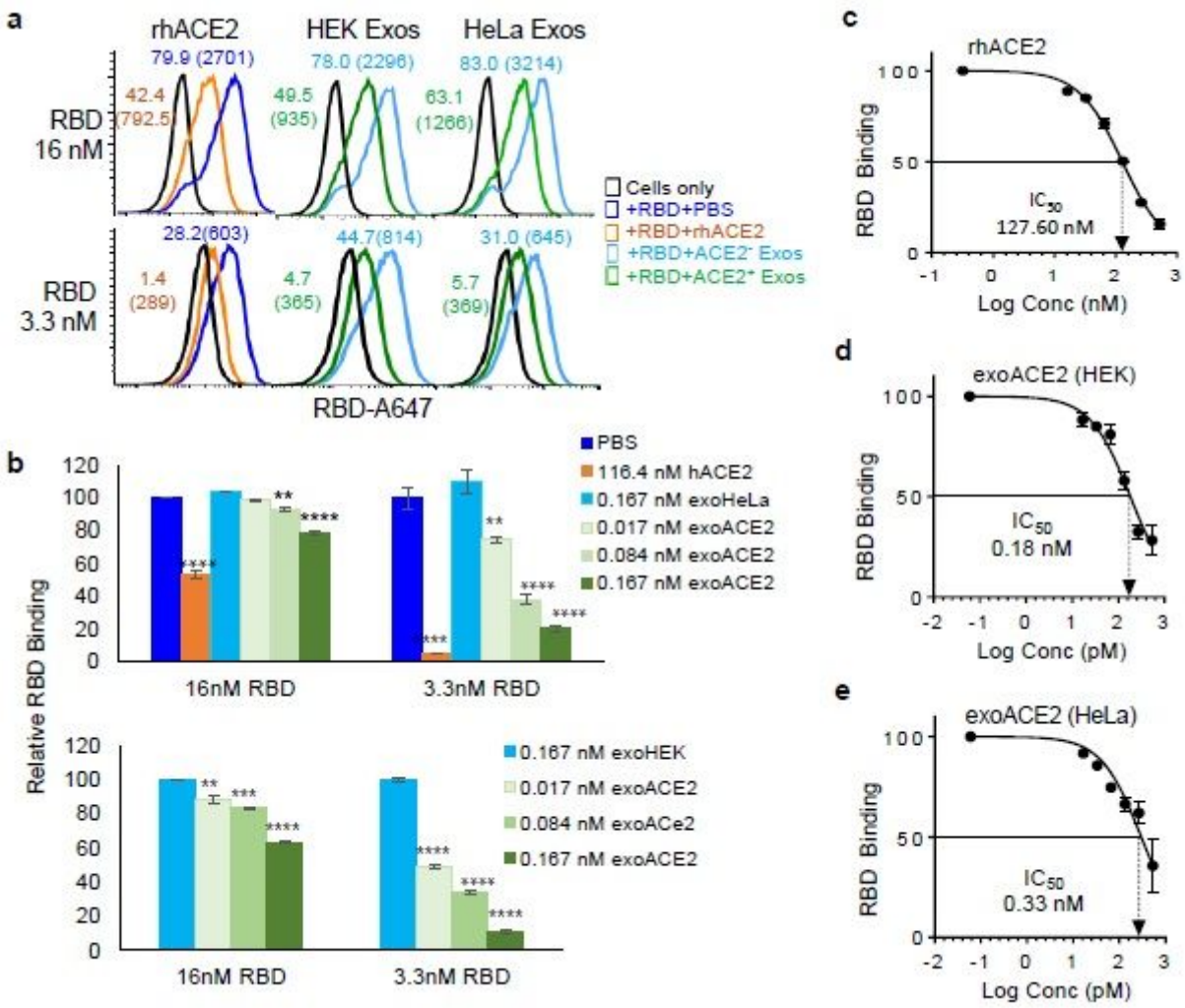

Figure 2

Neutralization effects of ACE2+ exosomes on RBD-binding to human host cells a. Flow profiles of RBD binding inhibited by rhACE2 and ACE2+ exosomes from HEK-293 and HeLa cells whereas ACE2- exosomes had minimal effects. b. Histogram bars of quantified RBD-neutralization by ACE2+ exosomes in a dose dependent manner (**p<0.01, ***p<0.001 and ****p<0.0001 compared to PBS or HEK Exos). c-e. IC50 of rhACE2 and exosomal ACE2 (exoACE2) in the exosomes from ACE2+ HEK and HeLa cells on 16 nM RBD-host cell binding (%).

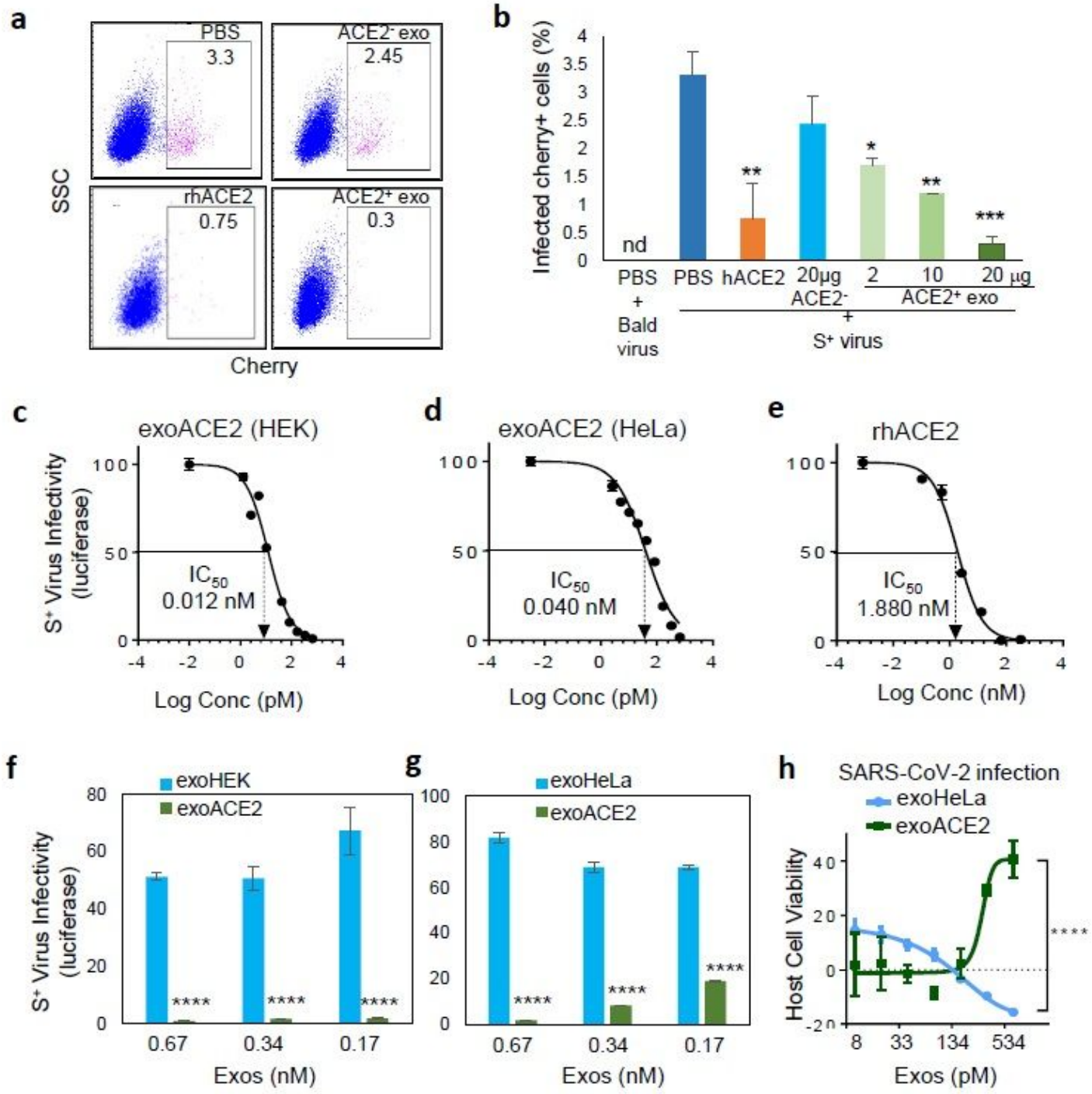

Figure 3

ACE2+ exosomes inhibit SARS-CoV-2 S+ pseudovirus infection to human host cells. a-b. Flow plots (a) and bar graph (b) of pseudovirus-infected HeLa-ACE2 cells, detected with Cherry reporter expression which was inhibited by rhACE2 and ACE2+ exosomes, but not ACE2- exosomes (nd= non-detectable, *p<0.05, **p<0.01 and ***p<0.001 compared to BS+Spike+). c-e. IC50 of exosomal ACE2 (exoACE2) in ACE2+ exosomes from HEK and HeLa cells and rhACE2. f-g. Luciferase-based SARS-COV-2 S+ pseudotype infectivity of HeLa-ACE2 cells in the presence of ACE2- and ACE2+ exosomes from both HEK (f) and HeLa (g) cells (****p<0.0001 compared to respective ACE2- exosomes). h. Vero-6 cell viability

upon wild-type SARS-CoV-2 infection which is partially protected by ACE2+ HeLa exosomes whereas ACE2- had no effects (****p<0.0001).

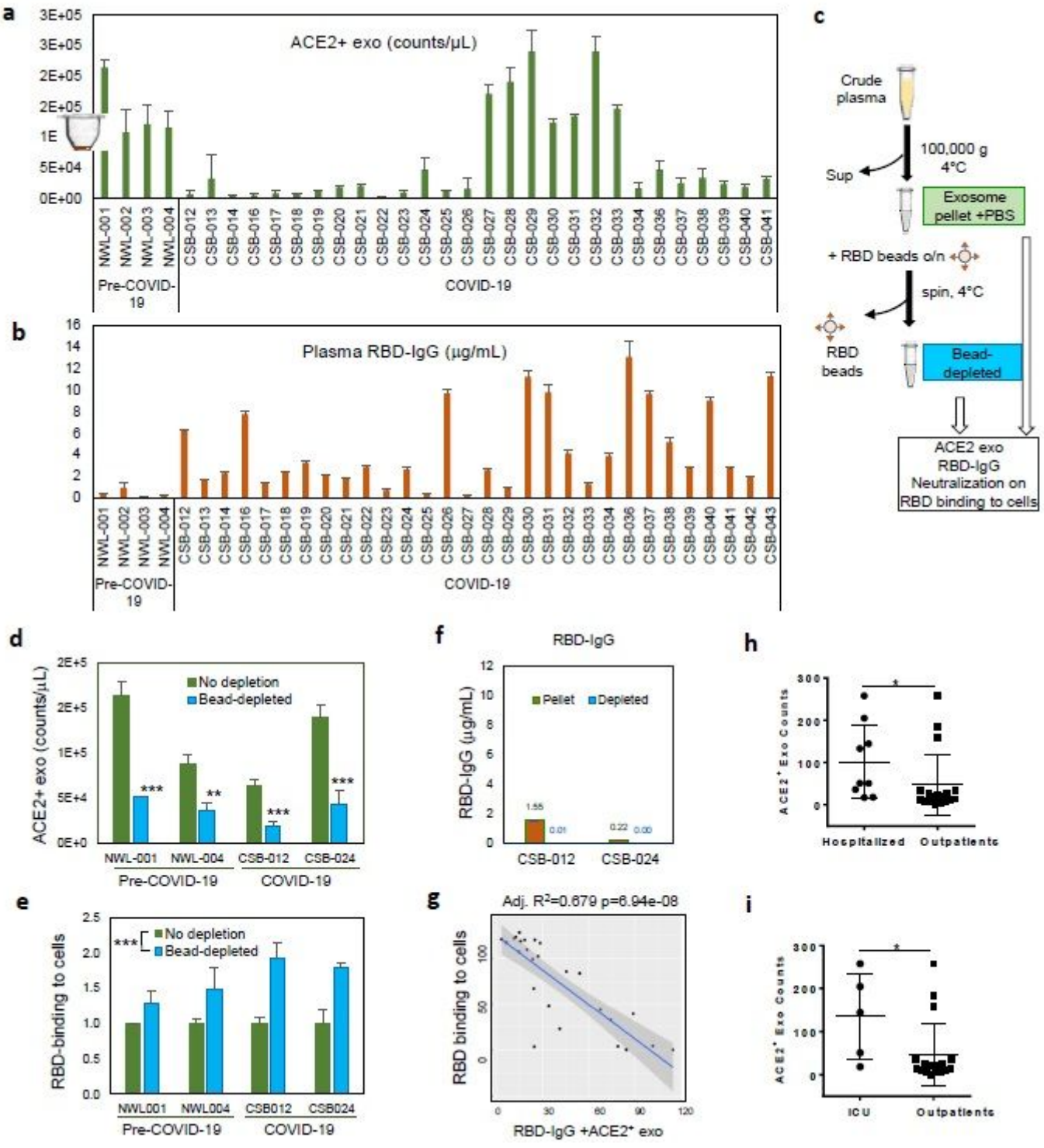

Figure 4

Detection of ACE2+ exosomes in NWL and CSB patient plasma. a-b. MFV counts of ACE2+ exosomes and ELISA-measured RBD-IgG levels in patient plasma, pre-COVID-19 (NWL) and convalescent COVID-19 plasma (CSB) c. Schematic of exosome enrichment and RBD-beads based depletion. d-e. Levels of ACE2+ exosome counts (d) and altered RBD-host cell binding (e) of the plasma exosome pellet prior to

and after RBD-bead depletion. **p<0.01, ***p<0.001. f. RBD-bead depletion reduced the residual RBD-IgG cells. g. Negative association of RBD binding to host cells with the integrated RBD-IgG and ACE2+ exosome levels in the convalescent COVID-19 patient plasma (N=30). h-i. ACE2+ exosomes positively associated with hospitalized (h) or ICU patients (i). *Ttest (tail 1, type 2) p<=0.05.

Supplementary Files

This is a list of supplementary files associated with this preprint. Click to download.

- SupplementaryFigures.pdf